scientific reports

OPEN

Parametric estimation of gyrotactic microorganism hybrid nanofluid flow between the conical gap of spinning disk-cone apparatus

Hussam Alrabaiah[1,2], Muhammad Bilal[3], Muhammad Altaf Khan[4], Taseer Muhammad[5] & Endris Yimer Legas[6]✉

The silver, magnesium oxide and gyrotactic microorganism-based hybrid nanofluid flow inside the conical space between disc and cone is addressed in the perspective of thermal energy stabilization. Different cases have been discussed between the spinning of cone and disc in the same or counter wise directions. The hybrid nanofluid has been synthesized in the presence of silver *Ag* and magnesium oxide *MgO* nanoparticulate. The viscous dissipation and the magnetic field factors are introduced to the modeled equations. The parametric continuation method (PCM) is utilized to numerically handle the modeled problem. Magnesium oxide is chemically made up of Mg^{2+} and O^{2-} ions that are bound by a strong ionic connection and can be made by pyrolyzing $Mg(OH)^2$ (magnesium hydroxide) and $MgCO^3$ (magnesium carbonate) at high temperature (700–1500 °C). For metallurgical, biomedical and electrical implementations, it is more efficient. Similarly, silver nanoparticle's antibacterial properties could be employed to control bacterial growth. It has been observed that a circulating disc with a stationary cone can achieve the optimum cooling of the cone-disk apparatus while the outer edge temperature remains fixed. The thermal energy profile remarkably upgraded with the magnetic effect, the addition of nanoparticulate in base fluid and Eckert number.

Abbreviations

r	Radial distance
c	Constant
Nu_d	Nusselt number of cone
T	Fluid temperature (K)
T_∞	Ambient temperature
Pr	Prandtl number
M	Magnetic number
$Re_\Omega = r^2\Omega/v$	Local Reynold number
(r, φ, z)	Cylindrical coordinate
u, v, w	Velocity component
n	Surface temperature power index
Nu_d	Nusselt number of disk
T_w	Surface temperature
$p(\text{Pa})$	Pressure
Ec	Eckert number
B_0	Magnetic field
$Re_\omega = r^2\omega/v$	Local Reynold number
F, G, H	Dimensional velocity

[1]College of Engineering, Al Ain University, Al Ain, United Arab Emirates. [2]Department of Mathematics, Tafila Technical University, Tafila, Jordan. [3]Department of Mathematics, City University of Science and Information Technology, Peshawar, Pakistan. [4]Institute for Groundwater Studies, Faculty of Natural and Agricultural Sciences, University of the Free State, Bloemfontein, South Africa. [5]Department of Mathematics, College of Sciences, King Khalid University, Abha 61413, Saudi Arabia. [6]Department of Mathematics, College of Natural Science, Wollo University, Dessie, Ethiopia. ✉email: fitsumeabee@gmail.com

1

Greek symbols

η	Similarity variable
ν	Kinematic viscosity (m^2 s^{-1})
ω	Angular velocity of disk (r s^{-1})
Θ	Dimensionless temperature
k_{nf}	Thermal conductivity (Wm^{-1} K^{-1})
$\phi_{Fe_3O_4}$	Iron oxide volume fraction
k_{hnf}	Thermal conductivity
σ	Electrical conductivity (S/m)
ρ_{hnf}	Hybrid Nanofluid density
η_0	Cone surface
μ	Dynamic viscosity (kg m^{-1} s^{-1})
μ_{hnf}	Dynamic viscosity of nanofluid
$(\rho c_p)_{hnf}$	Heat capacitance of hybrid nanoliquid (kg m^2 s^{-2} K^{-1})
Ω	Angular velocity of cone (r s^{-1})
ϕ_{Cu}	Copper volume fraction
α	Thermal diffusivity (m^2 s^{-1})
γ	Gap angle (°)
ν_{hnf}	Nanofluid kinematic viscosity

The analysis illustrates that disk-cone devices have a variety of technical and practical implementations, including Oldroyd-B fluid stability analysis, estimation of fluid viscosity, medical requirement, the cooling system of the conical diffuser, convective propagation of feeding culture and in biomedicine[1]. Turkyilmazoglu et al.[2] revealed the solution for constant an incompressible Newtonian fluid flow over a spinning cone using an analytical strategy. Chamkha and Mudhaf[3] examined the mass and energy transition over a vertical impermeable cone circulating with an unsteady angular velocity in an ambient fluid in the presence of heat absorption or generation and magnetic reactions. When the angular acceleration of the cone improves, the azimuthal and tangential skin-friction factors, as well as the Sherwood and Nusselt numbers improve. In the context of thermal energy radiation, the phenomenon of magnetic nanoliquid flow across a revolving cone has been considered by Nadeem[4]. According to the results of the investigation, the magnetic parameter M reduces velocity in both secondary and primary directions. Gul et al.[5] reported a 3D Darcy MHD Casson fluid, continuous flow across the gap of spinning disc and cone. It has been discovered that as the Peclet and Lewis numbers improve, the motile density of microbes reduces. Li et al.[6,7] addressed the viscous fluids flow due to a spinning cone and disk. For greater variable viscosity parameters, temperature and velocity exhibit divergent responses. Both entropy optimization and Bejan number have a comparable influence on the growing values of the thermal conductivity variable. Lv et al.[8] evaluated the Hall current, magnetic field, and heat radiation influenced nanofluids to flow on a revolving disk's surface. The goal of their effort was to improve heat conveyance rates for industrial and engineering applications. Ahmadian et al.[9,10] explored at a 3D computational model for Ag-MgO hybrid nanofluid flow with energy and mass transmission generated by an irregular fluctuating spinning disc. The configuration of a circulating disc is thought to have a favorable effect on thermal energy and velocity transmission.

Hybrid nanofluids are a unique type of fluid that operates well in energy translocation when compared to traditional fluids such as water and oil. When the heat intensity is high enough, nanofluids may be used in a wide range of thermal activities[11,12]. Hybrid nanofluid flow is used in a variety of applications, including heat exchangers, heat pipes, solar energy, manufacturing, automobile sector, air conditioning, generator cooling, nuclear system cooling, electronic cooling, ships, transformer cooling and biomedicine[13]. In this study, we examined the characteristics of silver and magnesium oxide nanostructures using water as a carrier fluid. Because of their distinctive chemical and physical features, Silver nanoparticles (AgNPs) are being used in a wide range of industries, including pharmaceuticals, foodstuff, consumption products, medical services, and manufacturing. Among these optical, thermal and electrical characteristics, as well as strong electrical conductivity and biological qualities[14]. Magnesium Oxide Nanoparticles (MgONPs) are an antimicrobial that is harmless and reasonably cheap to obtain. The United States Drug and Food Administration has approved MgONPs as non-toxic and safe chemicals (21CFR184.1431). Recent advancements in technologies and medicine have resulted in notable discoveries with great promise. MgONPs, for instance, can alleviate heartburn, activate bone healing scaffolds after they have been activated, and function as hyperthermia accelerators in cancer treatment[15]. Anuar et al.[16] evaluated the boundary layer flow and thermal performance of a hybrid nanoliquid including silver and magnesium oxide nanocomposites as it passed through an inclined stretching sheet with buoyant and suction force. The observations show that raising the quantity of Ag-MgO/water nanocrystals in nanofluid decreases the Nusselt number. Dinarvand et al.[17] used multiple approaches to investigate the constant laminar magnetohydrodynamics (MHD) flow of an Ag-MgO/water hybrid nanofluid across a lateral thin needle with heat radiation. Bilal et al.[18,19] addressed the relative contribution of magnetic and electric hydrodynamic effect on the water-based CNTs and iron oxide hybrid nanofluid flow between two circulating plates. Heat transfer has been assumed to rise as the magnetic field, electric term and Reynolds number improve. Sreedevi et al.[20] computationally evaluated the Ag-water-based radiative nanoliquid with fluid flow and heat transition characteristics within a circular tube with thermal conditions on vertical walls. When 0.05 volume fraction silver nanoparticles are dispersed in water, the heat transference rate improves from 6.3 to 12.4%. Zhao et al.[21] investigated the influence of viscous dissipation on the flow of a hybrid nanofluid across a stretched sheet utilising various nanoparticles to improve the fluid's thermal conductivity. Kumar et al.[22] studied the effect of activation energy on the Darcy–Forchheimer flow of Casson fluid using Graphene oxide and Titanium dioxide nanoparticle suspensions in a porous medium
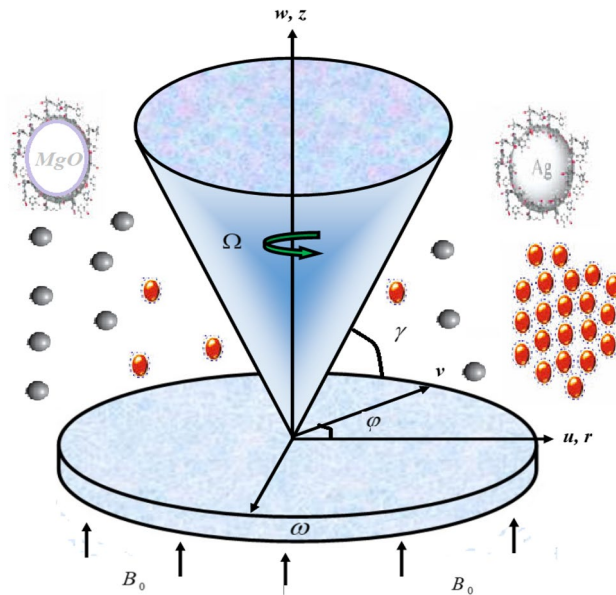
Figure 1. The hybrid nanofluid flow arrangement between the disc and cone.

using 50% Ethylene glycol as the base fluid. Khan et al.[23] presented about the Marangoni convection of a hybrid nanofluid made up of two nanoparticles and a base fluid. Some related literature may be found in[24–27].

Shi et al.[28,29] proposed a mathematical framework to evaluate the bio-convection flow of a magneto-cross nanofluid including gyrotactic microorganisms with transient magnetic flow of Cross nanoliquid through a stretched sheet. Yusuf et al.[30] studied the rate of entropy generation in a bio-convective flow of a MHD William-son nanoliquid across an inclined convectively heated stretchable plate, taking into account the effects of thermal radiation and chemical reaction. The presence of microorganisms has been shown to help in the stabilisation of suspended nanoparticles via a bioconvection mechanism. Khashi'ie et al.[31] and Wahid et al.[32] numerically investigates the influence of gyrotactic microorganisms in the mixed convection stagnation point flow of Cu-Al2O3/water hybrid nanofluid towards an immovable plate.

Highly nonlinear boundary value concerns that cannot be solved are common in the automotive industry. For many problems that are routinely addressed by other numerical methods, convergence is susceptible to relaxation constants and initial framework. The PCM's objective is to uncover the technique's universal applicability as a viable solution to nonlinear issues[33]. The 3D turbulent flow and heat transmission over the surface of an extensible spinning disc is highlighted by Shuaib et al.[34]. The fluid has been studied in the presence of external magnetic strength. Shuaib et al.[35] identified the characteristic of an ionic transitional boundary layer flow across a revolving disc. To find an ionic species, the Poisson's and Nernst-Planck equations were utilized. Wang et al.[36] used a parametric continuation technique to analyze the consistency of complex systems for engineering disciplines. They also investigated the static bifurcation that occurs while solving nonlinear starting value problems with distinct features and developed an algorithm for determining the bifurcation points in detail. Bilal et al.[37] explored the fluctuating Maxwell nanofluid flow around a stretched cylinder guided by suction/injection impact. The resulting system of ODEs was then numerically calculated using the PCM technique, and the results were validated using the Matlab program bvp4c.

The above examinations indicated that no attempt has been made so far to analyze the 3D flow of silver, magnesium oxide and gyrotactic microorganism-based hybrid nanofluid inside the conical space between disc and cone in perspective of thermal energy stabilization. Multiple cases involving the rotation of disc and cone in the same or reverse trajectory have been addressed. The hybrid nanocomposites are formed in the context of silver *Ag* and magnesium oxide MgO nanomaterials. The magnetic field and viscous dissipation components are included in the simulated equations. To numerically address the posed situation, the computational methodology parametric continuation method is used.

Mathematical formulation

We considered an incompressible flow of silver and magnesium oxide-based hybrid nanofluid between a cone and disk under the consequences of the magnetic field. The motile microorganism has been also considered in the present analysis. Both the devices are supposed to be either stationary or spinning in the r, φ, z direction (cylindrical coordinate) with the angular velocity. The Ω and ω elaborate the cone and disk angular velocities. Figure 1 communicates the hybrid nanofluid flow mechanism between the disk and cone. The phenomena. The radial variable surface temperature $T_w = T_\infty + cr^n$, where c and n are kept constant. Here, p is the pressure depends on radial r and axial z distance between the conical gaps. Based on the above presumption, the flow mechanism can be stated as[38]:

$$\frac{\partial u}{\partial r} + \frac{u}{r} + \frac{\partial w}{\partial z} = 0, \tag{1}$$

$$\rho_{hnf}\left(u\frac{\partial u}{\partial r} - \frac{v^2}{r} + w\frac{\partial u}{\partial z}\right) = -\frac{\partial p}{\partial r} + \mu_{hnf}\left(\frac{\partial^2 u}{\partial r^2} + \frac{1}{r}\frac{\partial u}{\partial r} - \frac{u}{r^2} + \frac{\partial^2 u}{\partial z^2}\right) - \sigma_{hnf}B_0^2 u, \tag{2}$$

$$\rho_{hnf}\left(u\frac{\partial v}{\partial r} + \frac{uv}{r} + w\frac{\partial v}{\partial z}\right) = \mu_{hnf}\left(\frac{\partial^2 v}{\partial r^2} + \frac{1}{r}\frac{\partial v}{\partial r} - \frac{v}{r^2} + \frac{\partial^2 v}{\partial z^2}\right) - \sigma_{hnf}B_0^2 v, \tag{3}$$

$$\rho_{hnf}\left(u\frac{\partial w}{\partial r} + w\frac{\partial w}{\partial z}\right) = -\frac{\partial p}{\partial z} + \mu_{hnf}\left(\frac{\partial^2 w}{\partial r^2} + \frac{1}{r}\frac{\partial w}{\partial r} + \frac{\partial^2 w}{\partial z^2}\right), \tag{4}$$

$$(\rho c p)_{hnf}\left(u\frac{\partial T}{\partial r} + w\frac{\partial T}{\partial z}\right) = k_{hnf}\frac{\partial^2 T}{\partial z^2} + \mu_{hnf}\left[\left(\frac{\partial u}{\partial z}\right)^2 + \left(\frac{\partial v}{\partial z}\right)^2\right] + \sigma_{hnf}B_0^2(u^2 + v^2), \tag{5}$$

$$\left(u\frac{\partial C}{\partial r} + w\frac{\partial C}{\partial z}\right) = D_{hnf}\frac{\partial^2 C}{\partial z^2}, \tag{6}$$

$$\left(w\frac{\partial \tilde{N}}{\partial z} + \tilde{w}\frac{\partial \tilde{N}}{\partial z} + \tilde{N}\frac{\partial \tilde{w}}{\partial z}\right) = D_n\frac{\partial^2 \tilde{N}}{\partial z^2}. \tag{7}$$

Here, Eq. (1) is the continuity equation, Eqs. (2)–(4) are the momentum equations along u, v and w direction. Where, Eq. (5) represents energy transition rate, Eqs. (6) and (7) introduced concentration and motile microorganism profiles respectively. Here, $\tilde{N}$, D_n, Wc, B_0 and p is the motile microorganism's density, microorganism diffusion, floating velocity of cell, magnetic strength and pressure. While $k_{hnf}, v_{hnf}, \rho_{hnf}, \mu_{hnf}, (\rho c_p)_{hnf}$ and (u, v, w) is the thermal conductivity, kinematic viscosity, density, dynamic viscosity, electrical conductivity, heat capacitance and velocity terms along r, φ, z direction.

The boundary conditions are:

$$\begin{aligned} u = 0, \; v = \omega r, \; w = 0, \;\; C = C_w, \; \tilde{N} = \tilde{N}_w, \;\; T = T_w \text{ at } z = 0 \\ u = 0, \; v = \Omega r, \; w = 0, \;\; C = C_\infty, \; \tilde{N} = \tilde{N}_\infty, \;\; T = T_\infty \text{ at } z = r\tan\gamma \end{aligned} \tag{8}$$

Here γ specified the gap angle between the cone and disk.

Similarity conversion. We adopt the following similarity transformation[39]:

$$u = \frac{\upsilon_f}{r}f(\eta), \; v = \frac{\upsilon_f}{r}g(\eta), \; w = \frac{\upsilon_f}{r}h(\eta), \; p = \frac{\rho\upsilon_f^2}{r^2}P, \;\; \eta = \frac{z}{r}, \;\; \Theta = \frac{T - T_\infty}{T_w - T_\infty}, \; \lambda = \frac{N - N_\infty}{N_w - N_\infty}, \;\; \Phi = \frac{C - C_\infty}{C_w - C_\infty}. \tag{9}$$

Using Eqs. (8) in Eqs. (2–5), we get:

$$h' = \eta f', \tag{10}$$

$$(1 + \eta^2)f'' = -3\eta f' - D_1 A_1(\eta f f' - h f' + f^2 - g^2) - D_1(2p + \eta p' - Mf), \tag{11}$$

$$(1 + \eta^2)g'' = D_1 B_1(\eta f g' - h g') + D_1 g M - 3\eta g', \tag{12}$$

$$(1 + \eta^2)h'' = -3\eta h' - D_1 A_1(\eta f h' - h h' + h + f h) + D_1 p', \tag{13}$$

$$\frac{k_{hnf}}{k_{nf}}\left((1 + \eta^2)\Theta'' = -\eta(1 - 2n)\Theta' + n^2\Theta\right) - C_1 Pr(\eta f\Theta' - h\Theta' - nf\Theta) - ((f')^2 + (g')^2)Ec \\ -\frac{MEc}{D_1}(f^2 + g^2), \tag{14}$$

$$(1 + \eta^2)D_1 \Phi'' = Sc(f\Phi'), \tag{15}$$

$$\lambda'' = -\text{Re}(2Scf\lambda' + Pe(\lambda'\Phi' - \lambda\Phi'')). \tag{16}$$

where,

$$A_1 = \left[(1-\phi_{MgO})\left(1-\left(1-\frac{\rho_{Ag}}{\rho_f}\right)\phi_{Ag}\right)+\phi_{MgO}\left(\frac{\rho_{MgO}}{\rho_f}\right)\right], B_1 = \left[\begin{array}{c}(1-\phi_{Cu})\left(1-\left(1-\frac{\rho_{Ag}}{\rho_f}\right)\phi_{Ag}\right)\\+\phi_{MgO}\left(\frac{\rho_{MgO}}{\rho_f}\right)\end{array}\right],$$

$$C_1 = \left[(1-\phi_{MgO})\left(1-\left(1-\frac{(\rho C_p)_{Ag}}{(C_p\rho)_f}\right)\phi_{Ag}+\frac{(\rho C_p)_{MgO}}{(C_p\rho)_f}\phi_{MgO}\right)\right], D_1 = (1-\phi_{Ag})^{2.5}(1-\phi_{MgO})^{2.5}.$$

(17)

The modified conditions are:

$$f(0)=0,\ g(0)=Re_\omega,\ h(0)=0,\ \Theta(0)=1,\ \Phi(0)=1,\ \check\lambda(0)=1,$$
$$f(\eta_0)=0,\ g(\eta_0)=Re_\Omega,\ h(\eta_0)=0,\ \Theta(\eta_0)=0,\ \Phi(\eta_0)=0,\ \check\lambda(\eta_0)=0.$$

(18)

The volumetric fraction of *Ag* and *MgO* are demonstrated through ϕ_{Ag} and ϕ_{MgO}. While $k_{hnf}\,k_f$ is the thermal conductivity of hybrid nanoliquid and water.

Thermo-physical properties. The following are the thermal properties of hybrid nanofluid and water are[42]:

$\upsilon_{hnf}=\frac{\mu_{hnf}}{\rho_{hnf}}$,	$\mu_{hnf}=\frac{\mu_f}{(1-\phi_{Ag})^{5/2}(1-\phi_{MgO})^{5/2}}$,
$\frac{(\rho)_{hnf}}{(\rho)_f}=(1-\phi_{MgO})\left(1-\left(1-\frac{\rho_{Ag}}{\rho_f}\right)\phi_{Ag}\right)+\phi_{MgO}\left(\frac{\rho_{MgO}}{\rho_f}\right)$,	
$\frac{(\rho C_p)_{hnf}}{(\rho C_p)_f}=(1-\phi_{MgO})\left\{1-\left(1-\frac{(\rho C_p)_{Ag}}{(\rho C_p)_f}\right)\phi_A\right\}+\frac{(\rho C_p)_{MgO}}{(\rho C_p)_f}\phi_{MgO}$,	
$\frac{k_{hnf}}{k_{nf}}=\frac{k_{MgO}+2k_{nf}-2\phi_{MgO}(k_{nf}-k_{MgO})}{k_{MgO}+2k_{nf}+\phi_{Cu}(k_{nf}-k_{MgO})}$,	
$\frac{k_{nf}}{k_f}=\frac{k_{Ag}+2k_f-2\phi_{Ag}(k_f-k_{Ag})}{k_{Ag}+2k_f+\phi_{Ag}(k_f-k_{Ag})}$.	

The dimensionless form of cone and disk are rebound as:

$$Nu_d = -\frac{k_{hnf}}{k_{nf}}\Theta'(0), Nu_c = -\frac{k_{hnf}}{k_{nf}}\Theta'(\eta_0).$$

(19)

Parametric continuation method
The basic idea of application of PCM method, to the system of ODE (10)–(17) with the boundary condition (18), is presented with the following steps[43]:

Step 1: We put forward the following submission to transfigure the system of BVP to the first-order ODE:

$$\left.\begin{array}{l}\ell_1=f(\eta),\ \ell_2=f'(\eta),\ \ell_3=g(\eta),\ \ell_4=g'(\eta),\ \ell_5=h(\eta),\ \ell_6=h'(\eta),\ \ell_7=p(\eta),\\\ell_8=\Theta(\eta),\ \ell_9=\Theta'(\eta),\ \ell_{10}=\Phi(\eta),\ \ell_{11}=\Phi'(\eta),\ \ell_{12}=\check\lambda(\eta),\ \ell_{13}=\check\lambda'(\eta).\end{array}\right\}$$

(20)

Using Eq. (20) in the BVP (10–16) and (18), we get:

$$\ell_5'=\eta\ell_2,$$

(21)

$$(1+\eta^2)\ell_2'=-3\eta\ell_2-A_1D_1(\eta\ell_1\ell_2-\ell_5\ell_2+\ell_1^2-\ell_3^2)-D_1(2\ell_7+\eta\ell_7+\eta\ell_7'-M\ell_1),$$

(22)

$$(1+\eta^2)\ell_4'=D_1B_1(\eta\ell_1\ell_4-\ell_5\ell_4)+D_1\ell_3M-3\eta\ell_4,$$

(23)

$$(1+\eta^2)\ell_6'=-3\eta\ell_6-D_1A_1(\eta\ell_1\ell_6-\ell_5\ell_6+\ell_5+\ell_1\ell_5+D_1\ell_7'),$$

(24)

$$(1+\eta^2)\ell_9'=-(\eta(1-2n)\ell_9+n^2\ell_8)-C_1Pr(\eta\ell_1\ell_8-n\ell_1\ell_8-\ell_5\ell_9)-Ec(\ell_2^2+\ell_4^2)-\frac{MEc}{D_1}(\ell_1^2+\ell_3^2),$$

(25)

$$(1+\eta^2)D_1\ell_{11}'=Sc(\ell_1\ell_{11}),$$

(26)

$$\ell_{13}'=-Re(2Sc\ell_1\ell_{12}+Pe(\ell_{13}\ell_{11}-\ell_{12}\ell_{11}')).$$

(27)

the reduced boundary conditions are:

$$\ell_1(0)=\ell_5(0)=0,\ \ell_3(0)=Re_\omega,\ \ell_8(0)=1,\ \ell_{10}(0)=1,\ \ell_{12}(0)=1,$$
$$\ell_1(\eta_0)=\ell_5(\eta_0)=0,\ \ell_3(\eta_0)=Re_\omega,\ \ell_8(\eta_0)=0,\ \ell_{10}(\eta_0)=0,\ \ell_{12}(\eta_0)=0.$$

(28)

Step 2: Introducing parameter p in Eqs. (25)–(30) as follow:

$$\ell_5' = \eta\ell_2 + \ell_5 - (\ell_5 - 1)p, \tag{29}$$

$$(1 + \eta^2)\ell_2' = -3\eta(\ell_2 - 1)p - A_1 D_1(\eta\ell_1\ell_2 - \ell_5\ell_2 + \ell_1^2 - \ell_3^2) - D_1(2\ell_7 + \eta\ell_7 + \eta\ell_7' - M\ell_1), \tag{30}$$

$$(1 + \eta^2)\ell_4' = D_1 B_1(\eta\ell_1(\ell_4 - 1)p - \ell_5\ell_4) + D_1\ell_3 M - 3\eta\ell_4, \tag{31}$$

$$(1 + \eta^2)\ell_6' = -3\eta\ell_6 - D_1 A_1(\eta\ell_1\ell_6 - \ell_5\ell_6 + \ell_5 + \ell_1\ell_5 + D_1\ell_7'), \tag{32}$$

$$(1 + \eta^2)\ell_9' = -(\eta(1 - 2n)(\ell_9 - 1)p + n^2\ell_8)$$
$$- C_1 Pr(\eta\ell_1\ell_8 - n\ell_1\ell_8 - \ell_5\ell_9) - Ec(\ell_2^2 + \ell_4^2) - \frac{MEc}{D_1}(\ell_1^2 + \ell_3^2), \tag{33}$$

$$(1 + \eta^2)D_1\ell_{11}' = Sc(\ell_1(\ell_{11} - 1)p), \tag{34}$$

$$\ell_{13}' = -Re(2Sc\ell_1\ell_{12} + Pe((\ell_{13} - 1)p\ell_{11} - \ell_{12}\ell_{11}')). \tag{35}$$

Step 3: Differentiating by parameter 'p'
While differentiating Eqs. (29–35) for parameter p, come at the following system in terms of parameter p:

$$V' = AV + R, \tag{36}$$

where R and A are the remainder and coefficient matrix respectively.

$$\frac{d\zeta_i}{d\tau} \tag{37}$$

where $i = 1, 2, \ldots 11$.

Step 4: Use the superposition approach to each problem and characterize the Cauchy problem

$$V = aU + W, \tag{38}$$

For each term, resolve the Cauchy problems below.

$$U' = aU, \tag{39}$$

$$W' = AW + R, \tag{40}$$

We obtained the estimated solution by putting Eq. (38) in Eq. (36).

$$(aU + W)' = A(aU + W) + R, \tag{41}$$

Step 5: Solving the Cauchy problems
This study employs a numerical implicit methodology, which is detailed below.

$$\frac{U^{i+1} - U^i}{\Delta\eta} = AU^{i+1}, \ or \ \ U^{i+1}(I - \Delta\eta A) = U^i, \tag{42}$$

$$\frac{W^{i+1} - W^i}{\Delta\eta} = AW^{i+1}, \ or \ \ W^{i+1}(I - \Delta\eta A) = W^i, \tag{43}$$

we get the iterative form of the solution.

$$U^{i+1} = (I - \Delta\eta A)^{-1}U^i, \tag{44}$$

$$W^{i+1} = (I - \Delta\eta A)^{-1}(W^i + \Delta\eta R). \tag{45}$$

Result and discussion

The goal of this part is to learn about the effects of velocity, temperature, mass, and motile microorganism distributions under the effect of multiple fundamental factors. The flow mechanics of a circulating cone and disc is observed in Fig. 1. Table 1 addressed the numerical properties of silver, magnesium oxide and water. The four different cases are discussed in detail between cone and disk. Case 1 elaborated that the disk is spinning while the cone is fixed. Case 2 revealed that the cone is spinning, while the disk is fixed. Case 3 & 4 highlighted that the disk and cone are co-rotating or counter-rotating respectively. The following observations have been noticed:

	$\rho(kg/m^3)$	$C_p(j/kgK)$	$k(W/mK)$	$\beta \times 10^5(K^{-1})$	Pr
Pure water	997.1	4179	0.613	21	6.2
Magnesium oxide	3560	955	45	1.80	
Silver	10,500	235	429	1.89	

Table 1. The numerical properties of silver, magnesium oxide and water[40,41].
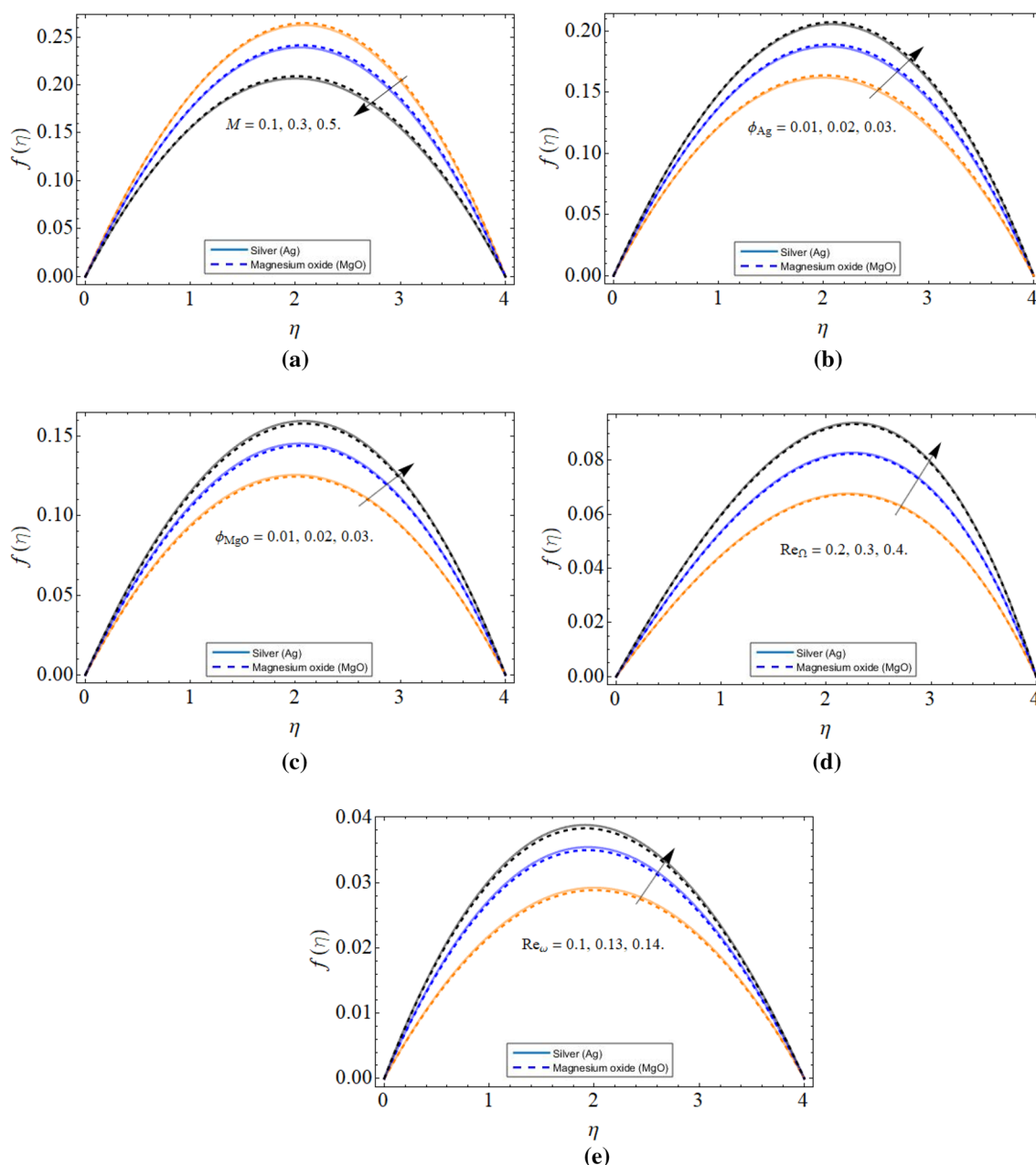
Figure 2. The behavior of axial velocity profile $f(\eta)$ versus (**a**) magnetic field M (**b**) volume friction of silver ϕ_{Ag} (**c**) volume friction of magnesium oxide ϕ_{MgO} (**d**) cone angular velocity Re_Ω (**e**) disk angular velocity Re_ω.

Axial velocity profile.   Figure 2a–e revealed the behavior of axial velocity $f(\eta)$ profile versus magnetic field M, volume friction of silver ϕ_{Ag}, volume friction of magnesium oxide ϕ_{MgO}, cone angular velocity Re_Ω and disk angular velocity Re_ω respectively. The resistive force generated due to the consequences of the magnetic field declines the axial velocity as shown in Fig. 2a. Figure 2b,c manifested that the velocity profile enhances with the increment of both silver Ag and magnesium oxide MgO nanomaterials because the specific heat capacity of MgO and Ag nanoparticles is much less than water, that's why the rising thermal energy inside the hybrid
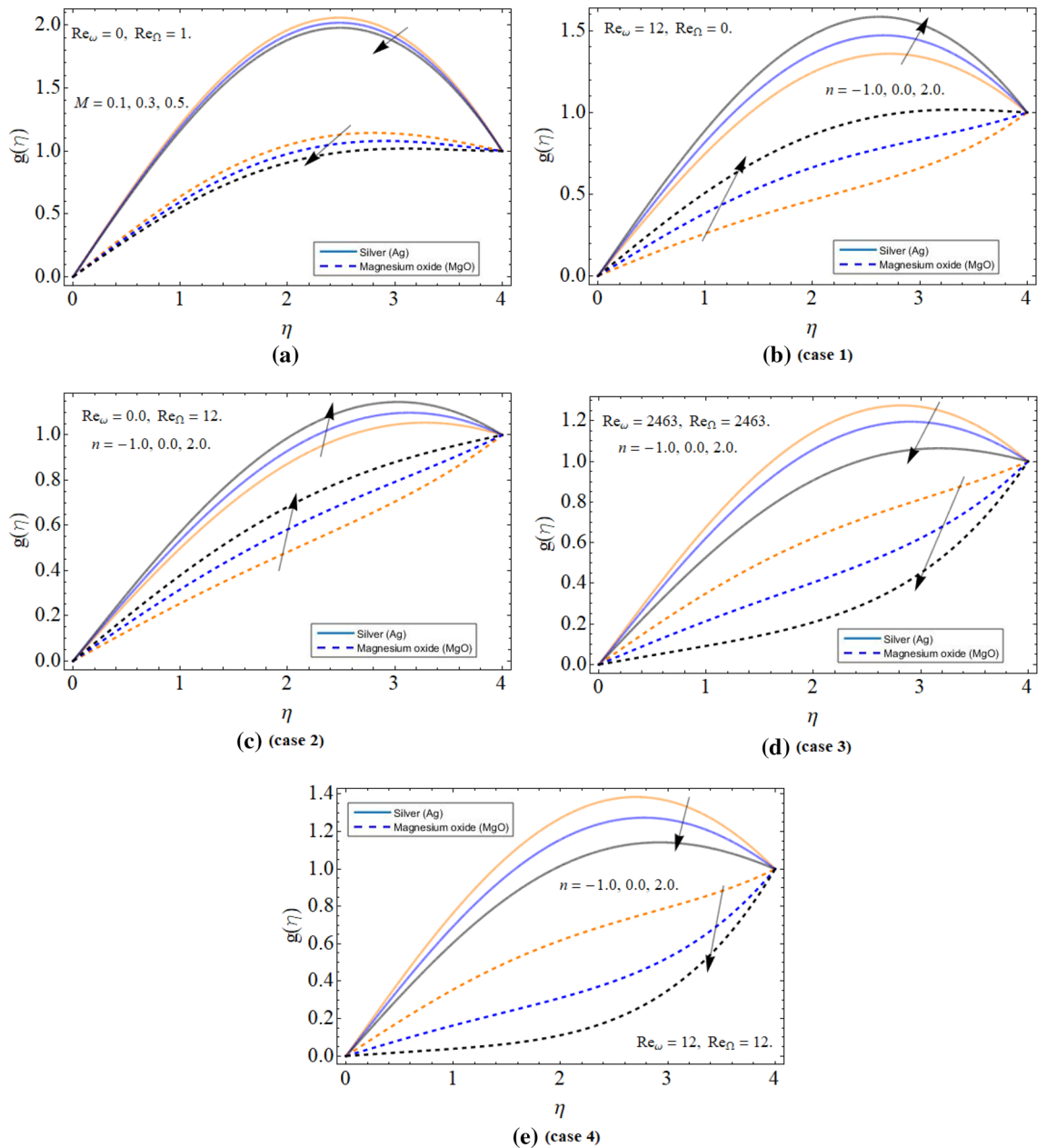
Figure 3. The behavior of radial velocity profile $g(\eta)$ versus (**a**) magnetic field M (**b**) disk rotation (**c**) cone rotation (**d**) both disk and cone co-rotation (**e**) both disk and cone counter rotation.

nanoliquid also causes the rises in fluid velocity. Figure 2d,e displayed that the velocity profile $f(\eta)$ significantly boosts with the growing values of both cone Ω and disk ω rotation. Physically, the improvement in both device's angular velocity encourages the fluid particles to move fast, which causes the inclination of axial velocity $f(\eta)$ across disk and cone.

Radial velocity profile. Figure 3a–e highlighted the behavior of radial velocity profile $g(\eta)$ versus magnetic field and four different cases of rotation and counter-rotation of both cone and disk respectively. The magnetic effect is also reducing the radial velocity, while keeping disk stationery and cone moving as illustrated in Fig. 3a. Figure 3b,c highlighted the two cases (1 & 2) and pointed that the radial velocity increases in both cases. Physically, the increasing velocity of both apparatuses excited the fluid particles, which become the reason for the enhancement of the radial velocity profile $g(\eta)$. Figure 3d,e connived cases 3 & 4 and shows that the velocity distribution reduces in both cases. The counter-rotation of the disk and cone generated resistance to the flow field, which decline the velocity profile.

Tangential velocity profile. Figure 4a–e elaborated the nature of tangential velocity profile $h(\eta)$ versus magnetic field M, volume friction of silver ϕ_{Ag}, volume friction of magnesium oxide ϕ_{MgO}, cone angular velocity
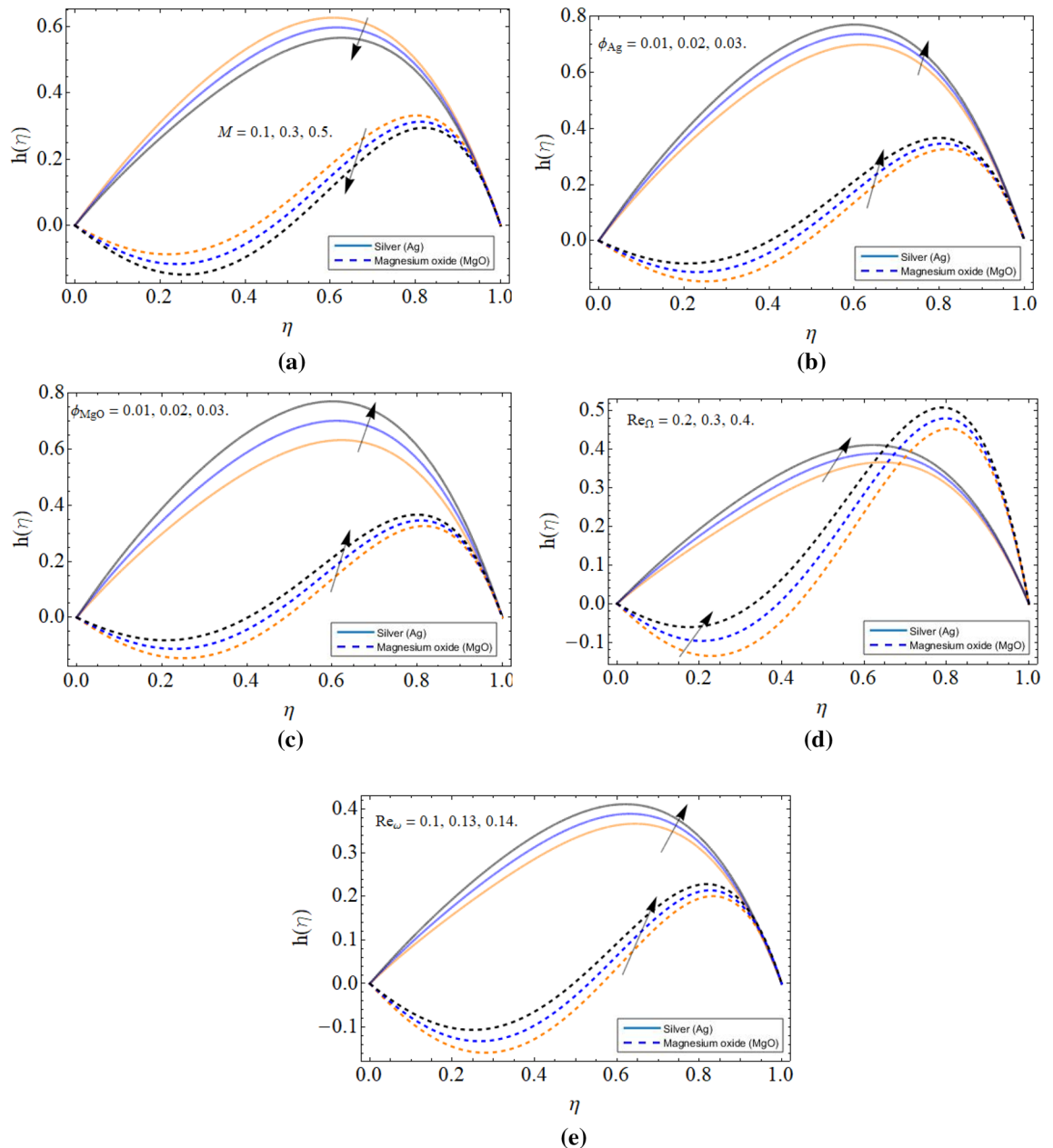
Figure 4. The behavior of tangential velocity profile $h(\eta)$ versus (**a**) magnetic field M (**b**) volume friction of silver ϕ_{Ag} (**c**) volume friction of magnesium oxide ϕ_{MgO} (**d**) cone angular velocity Re_Ω (**e**) disk angular velocity Re_ω.

Re_Ω and disk angular velocity Re_ω respectively. The tangential velocity of the fluid is significantly reducing with the influence of the magnetic field as shown in Fig. 4a. Figure 4b–e illustrated that the tangential velocity $h(\eta)$ profile boosts with the rising quantity of nanoparticles (Ag & MgO) and both disk Re_ω and cone Re_Ω increasing rotation respectively.

Thermal energy profile. Figure 5a–e displayed the characteristics of thermal energy profile $\Theta(\eta)$ versus magnetic field M, volume friction of silver ϕ_{Ag}, volume friction of magnesium oxide ϕ_{MgO}, Eckert number Ec and Prandtl number Pr respectively. Figure 5a–d communicated that the thermal energy profile remarkably upgraded with the magnetic effect, the addition of nanoparticulated in base fluid and Eckert number respectively. As we have discussed in Fig. 2b,c that the growing credit of nanoparticles diminishes the average specific heat capacity of base fluid, that's why such a scenario has been observed in Fig. 5b,c. Similarly, the dissipation energy is added to fluid internal energy and enhances its thermal energy $\Theta(\eta)$ distribution as exposed in Fig. 5d. The higher Prandtl fluid Pr has always less thermal diffusivity, that's why the Prandtl effect decrease fluid temperature $\Theta(\eta)$.
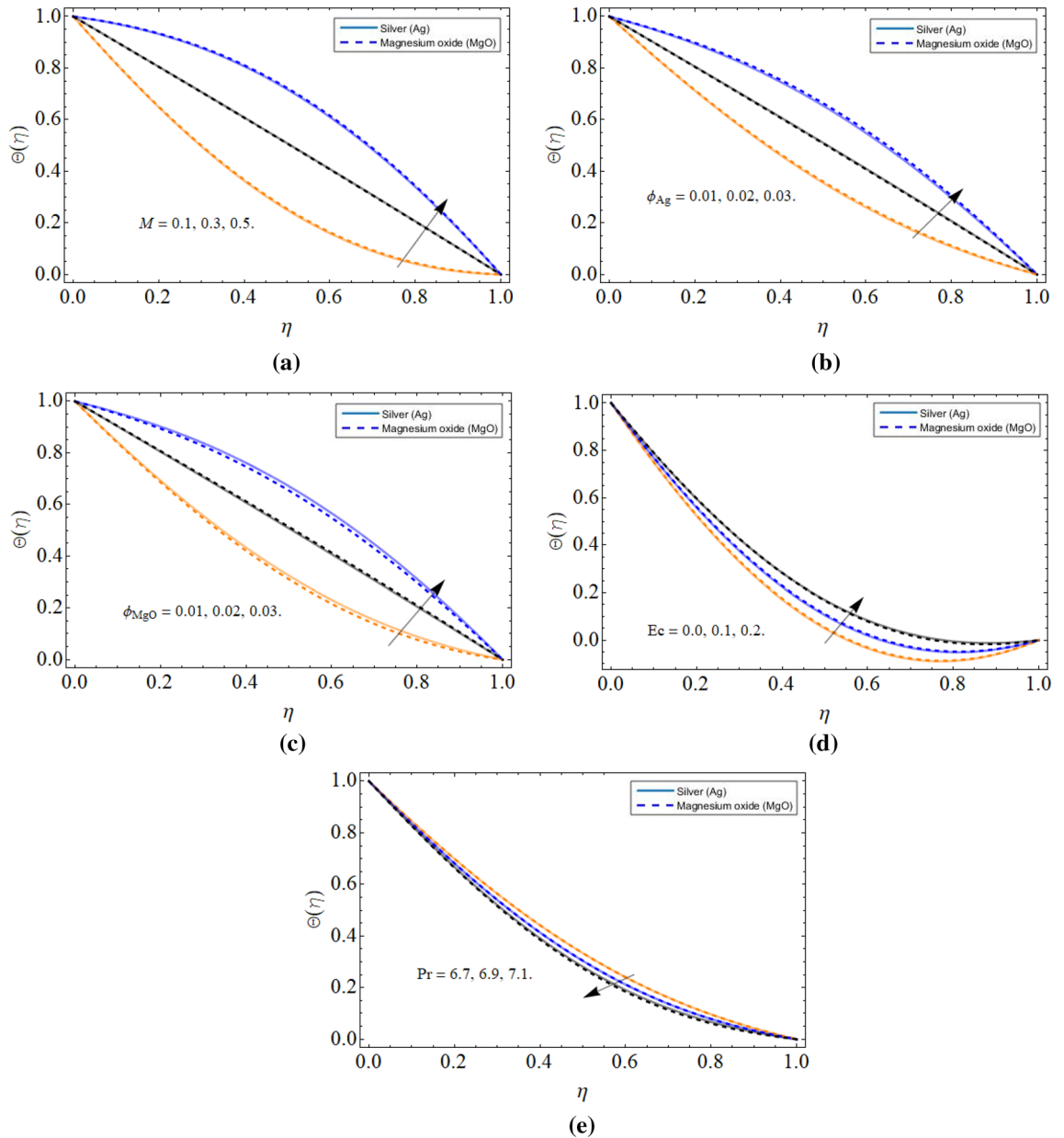
Figure 5. The behavior of thermal energy profile $\Theta(\eta)$ versus (**a**) magnetic field M (**b**) volume friction of silver ϕ_{Ag} (**c**) volume friction of magnesium oxide ϕ_{MgO} (**d**) Eckert number Ec (**e**) Prandtl number Pr.

Figure 6a–d spotted the four different cases between the cone and disk. The rotation of the disk, while keeping the cone fixed reduces the energy profile as appeared in Fig. 6a. An opposite scenario has been observed while keeping the disk fixed and spinning cone Fig. 6b. Figure 6c,d revealed that the energy profile reduces with the co-rotation of disk and cone, while enhances with counter-rotation because the opposite direction motion generates resistive force, which encourages fluid temperature $\Theta(\eta)$ as scrutinized in Fig. 6d.

Concentration and motile microorganism profile. Figure 7a–d manifested the behavior of mass transfer profile $\Phi(\eta)$ and motile microorganism $\lambda(\eta)$ versus Schmidt number Sc, volume friction of silver ϕ_{Ag}, Reynold number Re and Peclet number Pe respectively. The Schmidt number upshot diminished the mass transition rate as shown in Fig. 7a. Physically, the molecular diffusion lowers, and kinetic viscosity rises with Schmidt number, that's why such phenomena have been observed. An opposite scenario is observed against silver nanoparticles ϕ_{Ag} that the mass transference enhances with the upshot of silver nanoparticles as elaborated through Fig. 7b. Figure 7c,d illustrated that the bioconvection Reynold number Re and Peclet number Pe declines the motile microorganism $\lambda(\eta)$ profile. Because the density of microorganism decreases with the upshot of both Reynold number Re and Peclet number.
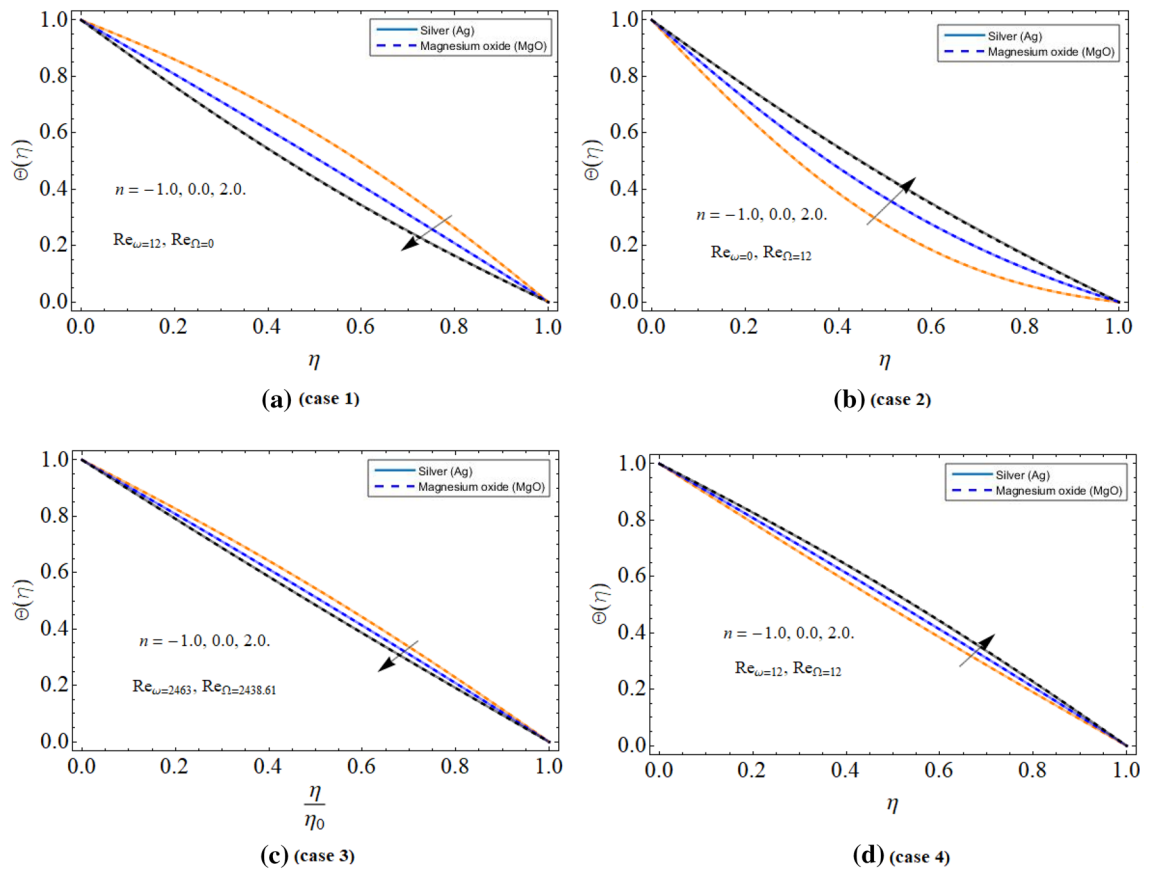
Figure 6. The behavior of thermal energy profile $\Theta(\eta)$ versus (**a**) disk rotation (**b**) cone rotation (**c**) both disk and cone co-rotation (**d**) both disk and cone counter-rotation.

Tables 2, 3, 4 and 5 exhibits the numerical results of the Nusselt number $-\Theta'(0)$ and Sherwood number $-\Phi'(0)$ at both, the disc surface and cone surface for the Ag and $Ag + MgO$ respectively. While Table 6 revealed comparative analysis for the validation of the results between PCM and bvp4c numerical Matlab package.

Conclusion

In the present study, the silver, magnesium oxide and gyrotactic microorganism-based hybrid nanofluid flow inside the conical space between disc and cone is addressed in the perspective of thermal energy stabilization. The hybrid nanofluid has been synthesized in the presence of silver Ag and magnesium oxide MgO nanoparticulate. The viscous dissipation and the magnetic field factors are introduced to the modeled equations. The numerical boundary value solver bvp4c is utilized to numerically handle the modeled problem. The following results have been observed:

- The resistive force generated due to the consequences of magnetic field declines the velocity profiles, while enhances with the increment of both silver Ag and magnesium oxide MgO nanomaterials.
- The velocity profile significantly boosts with the growing values of both cone Ω and disk ω rotation.
- The increasing velocity of both apparatuses (disk & cone) excited the fluid particles, which become the reason for the enhancement of velocity profiles.
- The fluid velocity boosts with the rising quantity of nanoparticles (Ag & MgO) and both disk Re_ω and cone Re_Ω increasing rotation.
- The thermal energy profile remarkably upgraded with the magnetic effect, the addition of nanoparticulated in base fluid and Eckert number respectively.
- The energy profile reduces with the co-rotation of disk and cone, while enhances with counter-rotation because the opposite direction motion generates resistive force, which encourages fluid temperature $\Theta(\eta)$.
- The motile microorganism profile decreases with the upshot of both Reynold number Re and Peclet number.
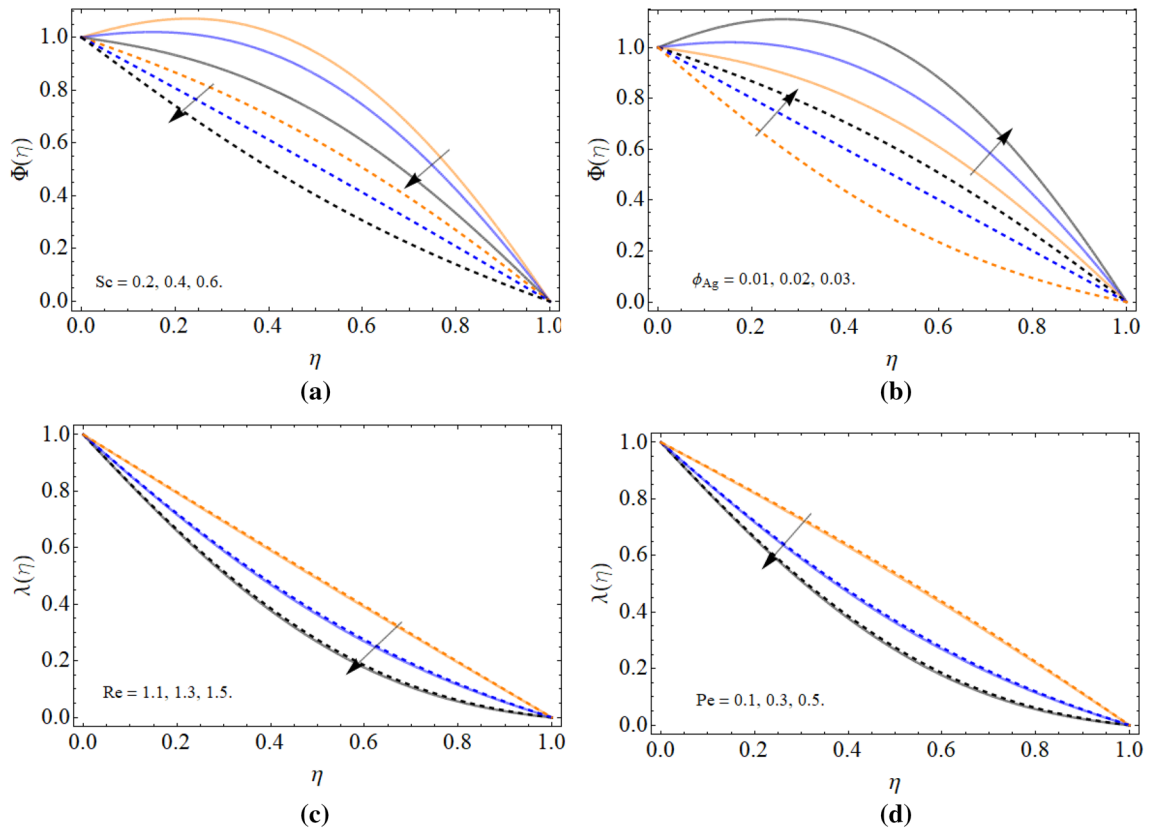
Figure 7. The behavior of mass transfer profile $\Phi(\eta)$ and motile microorganism $\lambda(\eta)$ versus (**a**) Schmidt number Sc (**b**) volume friction of silver ϕ_{Ag} (**c**) Reynold number Re (**d**) Peclet number Pe.

Pr	$-\Theta'(0)\ Ag$ $\phi_{Ag}=0.02$	$-\Theta'(0)\ Ag$ $\phi_{Ag}=0.04$	$-\Theta'(0)\ Ag+MgO$ $\phi_{Ag}=\phi_{MgO}=0.02$	$-\Theta'(0)\ Ag+MgO$ $\phi_{Ag}=\phi_{MgO}=0.04$
6.4	0.976487	0.979312	0.976945	0.981377
6.5	0.975697	0.979587	0.976274	0.979668
6.6	0.974928	0.978862	0.975492	0.969958

Table 2. Numerical outputs of Nusselt number $-\Theta'(0)$ at the surface of disc.

Pr	$-\Theta'(1)\ Ag$ $\phi_{Ag}=0.01$	$-\Theta'(1)\ Ag$ $\phi_{Ag}=0.02$	$-\Theta'(1)\ Ag+MgO$ $\phi_{Ag}=\phi_{MgO}=0.01$	$-\Theta'(1)\ Ag+MgO$ $\phi_{Ag}=\phi_{MgO}=0.02$
6.4	1.14573	1.24956	2.77864	2.78345
6.5	1.14487	1.23471	2.76196	2.77784
6.6	1.14367	1.22182	2.75845	2.76399

Table 3. Numerical outputs of Nusselt number $-\Theta'(1)$ at the surface of cone.

Sc	$-\Phi'(0)\ Ag$ $\phi_{Ag}=0.02$	$-\Phi'(0)\ Ag$ $\phi_{Ag}=0.04$	$-\Phi'(0)\ Ag+MgO$ $\phi_{Ag}=\phi_{MgO}=0.02$	$-\Phi'(0)\ Ag+MgO$ $\phi_{Ag}=\phi_{MgO}=0.04$
0.2	0.896487	0.899312	0.896945	0.891377
0.3	0.895697	0.899587	0.896274	0.899668
0.4	0.894928	0.898862	0.895492	0.899958

Table 4. Numerical outputs of Sherwood number $-\Phi'(0)$ at the surface of disc.

Sc	$-\Phi'(1)\,Ag$ $\phi_{Ag} = 0.01$	$-\Phi'(1)\,Ag$ $\phi_{Ag} = 0.02$	$-\Phi'(1)\,Ag + MgO$ $\phi_{Ag} = \phi_{MgO} = 0.01$	$-\Phi'(1)\,Ag + MgO$ $\phi_{Ag} = \phi_{MgO} = 0.02$
0.2	1.04573	1.04956	2.57864	2.58345
0.3	1.04487	1.03471	2.56196	2.57784
0.4	1.04367	1.02182	2.55845	2.56399

Table 5. Numerical outputs of Sherwood number $-\Phi'(1)$ at the surface of cone.

No.	PCM	bvp4c	Absolute Error
1	1.63×10^{-11}	6.325×10^{-17}	4.3298×10^{-14}
2	4.23×10^{-12}	3.834×10^{-20}	2.7139×10^{-15}
3	4.69×10^{-12}	2.8489×10^{-19}	4.6682×10^{-16}
4	7.429×10^{-14}	8.449×10^{-20}	7.6659×10^{-17}
5	6.898×10^{-14}	4.8378×10^{-20}	8.7392×10^{-17}

Table 6. PCM and bvp4c methods comparison for Ag: when $\phi_{Ag} = 0.04$, $\phi_{MgO} = 0.02$, $Pr = 6.3$, $Re_\Omega = 0.13$, $Re_\omega = 0.3$.

References

1. Spruell, C. & Baker, A. B. Analysis of a high-throughput cone-and-plate apparatus for the application of defined spatiotemporal flow to cultured cells. *Biotechnol. Bioeng.* **110**(6), 1782–1793 (2013).
2. Turkyilmazoglu, M. On the purely analytic computation of laminar boundary layer flow over a rotating cone. *Int. J. Eng. Sci.* **47**(9), 875–882 (2009).
3. Chamkha, A. J. & Al-Mudhaf, A. Unsteady heat and mass transfer from a rotating vertical cone with a magnetic field and heat generation or absorption effects. *Int. J. Therm. Sci.* **44**(3), 267–276 (2005).
4. Nadeem, S. Theoretical Investigation of MHD nanofluid flow over a rotating cone: An optimal solutions. *Inf. Sci. Lett.* **3**(2), 3 (2014).
5. Gul, T., Ahmed, Z., Jawad, M., Saeed, A. & Alghamdi, W. Bio-convectional nanofluid flow due to the thermophoresis and gyrotactic microorganism between the gap of a disk and cone. *Braz. J. Phys.* **51**(3), 687–697 (2021).
6. Li, Y. M. *et al.* An assessment of the mathematical model for estimating of entropy optimized viscous fluid flow towards a rotating cone surface. *Sci. Rep.* **11**(1), 1–15 (2021).
7. Li, Y. X. *et al.* Fractional simulation for Darcy-Forchheimer hybrid nanoliquid flow with partial slip over a spinning disk. *Alex. Eng. J.* **60**(5), 4787–4796 (2021).
8. Lv, Y. P. *et al.* Numerical approach towards gyrotactic microorganisms hybrid nanoliquid flow with the hall current and magnetic field over a spinning disk. *Sci. Rep.* **11**(1), 1–13 (2021).
9. Ahmadian, A., Bilal, M., Khan, M. A. & Asjad, M. I. Numerical analysis of thermal conductive hybrid nanofluid flow over the surface of a wavy spinning disk. *Sci. Rep.* **10**(1), 1–13 (2020).
10. Ahmadian, A., Bilal, M., Khan, M. A. & Asjad, M. I. The non-Newtonian maxwell nanofluid flow between two parallel rotating disks under the effects of magnetic field. *Sci. Rep.* **10**(1), 1–14 (2020).
11. Wahid, N. S., Arifin, N. M., Khashi'ie, N. S. & Pop, I. Marangoni hybrid nanofluid flow over a permeable infinite disk embedded in a porous medium. *Int. Commun. Heat Mass Transfer* **126**, 105421 (2021).
12. Madhukesh, J. K. *et al.* Numerical simulation of AA7072-AA7075/water-based hybrid nanofluid flow over a curved stretching sheet with Newtonian heating: A non-Fourier heat flux model approach. *J. Mol. Liquids* **335**, 116103 (2021).
13. Fisher, C., E Rider, A., Jun Han, Z., Kumar, S., Levchenko, I., & Ostrikov, K. K. Applications and nanotoxity of carbon nanotubes and graphene in biomedicine. *J. Nanomater.* (2012).
14. Zhang, X. F. Silver nanoparticles: Synthesis, characterization, properties, applications, and therapeutic approaches. *Int. J. Mol. Sci.* **17**, 1534 (2016).
15. Cai, L. *et al.* Magnesium oxide nanoparticles: Effective agricultural antibacterial agent against Ralstonia solanacearum. *Front. Microbiol.* **9**, 790 (2018).
16. Anuar, N. S., Bachok, N. & Pop, I. Influence of buoyancy force on Ag-MgO/water hybrid nanofluid flow in an inclined permeable stretching/shrinking sheet. *Int. Commun. Heat Mass Transfer* **123**, 105236 (2021).
17. Dinarvand, S., Mousavi, S. M., Yousefi, M., & Rostami, M. N. MHD flow of MgO-Ag/water hybrid nanofluid past a moving slim needle considering dual solutions: an applicable model for hot-wire anemometer analysis. *Int. J. Num. Methods Heat Fluid Flow* (2021).
18. Bilal, M. *et al.* Darcy-forchheimer hybrid nano fluid flow with mixed convection past an inclined cylinder. *CMC-Comput. Mater. Cont.* **66**, 2025–2039 (2021).
19. Bilal, M., Gul, T., Alsubie, A., & Ali, I. Axisymmetric hybrid nanofluid flow with heat and mass transfer amongst the two gyrating plates. *ZAMM J. Appl. Math. Mech.* e202000146 (2021).
20. Sreedevi, P., Reddy, P. S., & Suryanarayana Rao, K. V. Effect of magnetic field and radiation on heat transfer analysis of nanofluid inside a square cavity filled with silver nanoparticles: Tiwari–Das model. *Waves in Random and Complex Media*, 1–19 (2021).
21. Zhao, T. H. *et al.* Comparative study of ferromagnetic hybrid (manganese zinc ferrite, nickle zinc ferrite) nanofluids with velocity slip and convective conditions. *Phys. Script.* **96**(7), 5203 (2021).
22. Kumar, R. N., Gowda, R. P., Gireesha, B. J., & Prasannakumara, B. C. Non-Newtonian hybrid nanofluid flow over vertically upward/ downward moving rotating disk in a Darcy–Forchheimer porous medium. *Eur. Phys. J. Spec. Topics* 1–11 (2021).
23. Khan, M. I., Qayyum, S., Shah, F., Kumar, R. N., Gowda, R. P., Prasannakumara, B. C., ... & Kadry, S. Marangoni convective flow of hybrid nanofluid (MnZnFe2O4-NiZnFe2O4-H2O) with Darcy Forchheimer medium. *Ain Shams Eng. J* (2021).

24. Kumar, R. V., Gowda, R. P., Kumar, R. N., Radhika, M. & Prasannakumara, B. C. Two-phase flow of dusty fluid with suspended hybrid nanoparticles over a stretching cylinder with modified Fourier heat flux. *SN Appl. Sci.* **3**(3), 1–9 (2021).
25. Kumar, R. S., Alhadhrami, A., Gowda, R. J., Kumar, R. N., & Prasannakumara, B. C. Exploration of Arrhenius activation energy on hybrid nanofluid flow over a curved stretchable surface. *ZAMM-ZEITSCHRIFT FUR ANGEWANDTE MATHEMATIK UND MECHANIK* (2021).
26. Khashi'ie, N. S., Arifin, N. M., & Pop, I. Unsteady axisymmetric flow and heat transfer of a hybrid nanofluid over a permeable stretching/shrinking disc. *Int. J. Num. Methods Heat Fluid Flow* (2020).
27. Khashi'ie, N. S., Arifin, N. M., Merkin, J. H., Yahaya, R. I., & Pop, I. Mixed convective stagnation point flow of a hybrid nanofluid toward a vertical cylinder. *Int. J. Num. Methods Heat & Fluid Flow*. (2021).
28. Shi, Q. H. *et al.* Numerical study of bio-convection flow of magneto-cross nanofluid containing gyrotactic microorganisms with activation energy. *Sci. Rep.* **11**(1), 1–15 (2021).
29. Hamid, A., Khan, M. I., Kumar, R. N., Gowda, R. P., & Prasannakumara, B. C. Numerical study of bio-convection flow of magneto-Cross nanofluid containing gyrotactic microorganisms with effective Prandtl number approach (2021).
30. Yusuf, T. A., Mabood, F., Prasannakumara, B. C. & Sarris, I. E. Magneto-bioconvection flow of williamson nanofluid over an inclined plate with gyrotactic microorganisms and entropy generation. *Fluids* **6**(3), 109 (2021).
31. Khashi'ie, N. S., Arifin, N. M., Pop, I. & Nazar, R. Dual solutions of bioconvection hybrid nanofluid flow due to gyrotactic micro-organisms towards a vertical plate. *Chin. J. Phys.* **72**, 461–474 (2021).
32. Wahid, N. S. *et al.* Flow and heat transfer of hybrid nanofluid induced by an exponentially stretching/shrinking curved surface. *Case Stud. Thermal Eng.* **25**, 982 (2021).
33. Patil, A. A MODIFICATION and application of parametric continuation method to variety of nonlinear boundary value problems in applied mechanics. 2016.
34. Shuaib, M., Shah, R. A. & Bilal, M. Variable thickness flow over a rotating disk under the influence of variable magnetic field: An application to parametric continuation method. *Adv. Mech. Eng.* **12**, 1687814020936385 (2020).
35. Shuaib, M., Shah, R. A., Durrani, I. & Bilal, M. Electrokinetic viscous rotating disk flow of Poisson–Nernst–Planck equation for ion transport. *J. Mol. Liquids* **313**, 3412 (2020).
36. Dombovari, Z. *et al.* Experimental observations on unsafe zones in milling processes. *Philos. Trans. R. Soc. A* **377**, 125 (2019).
37. Bilal, M. *et al.* Comparative numerical analysis of Maxwell's time-dependent thermo-diffusive flow through a stretching cylinder. *Case Stud. Thermal Eng.* **1**, 101301 (2021).
38. Gul, T, Bilal, M., Alghamdi, W., Asjad, M. I. & Abdeljawad, T. Hybrid nanofluid flow within the conical gap between the cone and the surface of a rotating disk. *Sci. Rep.* **11**(1), 1–19 (2021).
39. Turkyilmazoglu, M. On the fluid flow and heat transfer between a cone and a disk both stationary or rotating. *Math. Comput. Simul.* **177**, 329–340 (2020).
40. Vajravelu, K. *et al.* Convective heat transfer in the flow of viscous Ag–water and Cu–water nanofluids over a stretching surface. *Int. J. Therm. Sci.* **50**(5), 843–851 (2011).
41. Davarnejad, R. & Jamshidzadeh, M. CFD modeling of heat transfer performance of MgO-water nanofluid under turbulent flow. *Eng. Sci. Technol. Int. J.* **18**(4), 536–542 (2015).
42. Gul, T. *et al.* Viscous dissipated hybrid nanoliquid flow with Darcy-Forchheimer and forced convection over a moving thin needle. *AIP Adv.* **10**(10), 105308 (2020).
43. Patil, A. *A modification and application of parametric continuation method to variety of nonlinear boundary value problems in applied mechanics*. Rochester Institute of Technology (2016).

Author contributions

Competing interests

The authors declare no competing interests.

Additional information

Correspondence and requests for materials should be addressed to E.Y.L.

Reprints and permissions information is available at www.nature.com/reprints.

Publisher's note Springer Nature remains neutral with regard to jurisdictional claims in published maps and institutional affiliations.